Synchrotron x-ray and optical studies of the structure of HgSe semiconductor nanoclusters confined in zeolite L and zeolite Y

A. M. M. Abeykoon,[1] M. Castro-Colin,[2] E. V. Anokhina,[3,*] M. N. Iliev,[4] W. Donner,[1] A. J. Jacobson,[5] and S. C. Moss[1]
[1]*Department of Physics, University of Houston, Houston, Texas 77204, USA*
[2]*Department of Physics, University of Texas, El Paso, Texas 79968, USA*
[3]*Department of Chemistry, University of Houston, Houston, Texas 77204, USA*
[4]*Texas Center for Superconductivity at the University of Houston (TcSUH), Houston, Texas 77204, USA*
[5]*Department of Chemistry/TcSUH, Houston, Texas 77204, USA*
(Received 10 July 2007; revised manuscript received 6 November 2007; published 28 February 2008)

HgSe semiconductor nanoclusters were fabricated in nearly spherical pores of zeolite Y and one-dimensional (1D) tubular pores of zeolite L. Anomalous x-ray scattering (AXS) data sets were collected on both HgSe/zeolite Y and HgSe/zeolite L systems, together with optical studies (Raman and UV-visible absorption). Two distinct structural models were determined by performing the Rietveld refinement on AXS data sets. Given the existence of a pronounced diffuse scattering in both filled zeolites and our refined models without the observed diffuse background, for each system, we propose the existence of an average HgSe nanocluster or a 1D nanostructure and the related disorder within the nanocluster which gives off the diffuse scattering. Optical studies were used to complement our x-ray structural work.

DOI: 10.1103/PhysRevB.77.075333 PACS number(s): 61.46.Df, 82.75.Vx, 61.05.C−, 78.70.Ck

I. INTRODUCTION

When electrons and holes in a semiconductor are confined to ultrasmall regions of space (typically 1–25 nm), the optical and electronic properties of the semiconductor become strongly size dependent. Such structures are called quantum dots, nanowires, or nanoclusters, depending on their shape and dimensionality. These nanostructures are of great interest for a variety of potential electronic, photochemical, and nonlinear optical applications.[1,2] Studying the atomic structures of these nanoclusters is necessary for an analysis of the transition from molecular to bulk semiconductor properties.

A variety of techniques such as colloidal, sol-gel, capping, nanocrystal doping, and porous host methods[1,3] are used to fabricate semiconductor nanoclusters today. However, most of these techniques do not permit to control the particle size easily and thereby produce nanoclusters with a narrow size distribution. This becomes a major disadvantage in the nanoscale regime, due to the strong size dependence of the optical and electronic properties of the semiconductors. Fabrication of semiconductor nanoclusters in a well-organized host matrix is a promising strategy to overcome this problem and to form semiconductor nanoclusters with a highly uniform shape and size distribution. This technique is based on the self-assembly of the nanoparticles and does not require expensive technology. Cheap availability of the host materials, such as polymers and molecular sieves, is another advantage associated with this method. However, when the fabrication of nanoclusters with a narrow size distribution is achieved using a well-organized framework, it is a challenge to find the atomic structure of the encapsulated species. Conventional x-ray and neutron diffraction,[4] anomalous x-ray scattering (AXS),[5] the pair distribution function (PDF) technique using synchrotron x rays or neutrons,[6] and Raman spectroscopy[4,7,8] are some of the techniques capable of extracting structural information from the encapsulate, knowing the structure of the host framework. However, according to the literature,[8–10] in most cases, the structure of the semiconductor nanoclusters confined within different types of host frameworks have been predicted using Raman spectroscopy or extended x-ray absorption fine structure studies, which provide limited structural information beyond the nearest few neighbors. AXS is a very powerful technique to obtain structural information beyond the nearest neighbor, especially when one phase is embedded in another. In this method, multiple x-ray diffraction (XRD) patterns are recorded, one at the vicinity (−20 eV) of the absorption edge of an element of interest and the other one far (±200 eV) from the absorption edges. The structure factor associated with the particular element can be determined by exploiting the difference in scattering power of the element at the two energies. As a result, the identity of the element at each site can ideally be attained. In addition, if there exists disorder within the encapsulate such as orientational or occupancy disorder, it will alter the intensities of the Bragg peaks and create a diffuse background,[11] under the Bragg peaks of the XRD pattern. In such cases, the PDF technique is capable of extracting additional structural information from the encapsulate. The diffuse scattering observed here cannot be explained by interpore correlations nor by the above intracore disorder.

The initial phase of this research was focused on the synthesis of the semiconductor nanoclusters with a precise, controllable, and narrow size distribution. Since zeolite frameworks severely constrain the size and shape of species encapsulated within a pore, zeolite pores were used to fabricate the semiconductor nanoclusters. Two zeolite frameworks, zeolite L (LTL structure so-called Linde type L, which contains 7.1 Å diameter tubular pores) and zeolite Y (faujasite structure, which contains 13 Å diameter nearly spherical pores) were chosen with the binary compound semiconductor HgSe for our study for several reasons: at least two sizes of nanoclusters are necessary for studying the size dependent properties of the semiconductors. Spherical

cages of zeolite Y permit quantum confinement in all three dimensions and production of the nanoclusters, while the LTL structure permits quantum confinement in two dimensions and fabrication of nanowire-type structures. Both nanostructures may have potential electronic applications such as nanowires, single electron logic memory elements, photonic crystals, etc.[12–14] Over recent years, a number of publications on the fabrication of semiconductor nanoclusters in zeolite pores including CdS(Se), Se, Rb-Se, and Cs-Se, in zeolite Y,[8,9,15,16] and Se, Pt, PbI_2, in LTL, have been reported.[18–20] However, to the best of our knowledge, the binary compound semiconductor HgSe has never been studied in the pores of zeolite L or zeolite Y.

The advantage of using a binary compound, in addition to its shape and size, is that it gives another variable, sample composition to control its properties, which, however, somewhat complicates the analysis. The scattering contrast between Hg and Se was another reason to choose this combination, using Se K (~12.65 keV) and Hg L (~12.29 keV) lines of the x-ray characteristic spectrum.

The goal of the second part of this work has been to find a successful structural model which may lead to a better understanding of the electronic properties of the nanoclusters. Atomic structures of the semiconductor nanoclusters were modeled using the AXS technique together with a Rietveld refinement of these AXS data using the GSAS/EXPGUI[21] computer package. These results were complemented by Raman spectroscopy and several other experimental techniques, such as optical absorption measurements and thermogravimetric analysis (TGA). We propose two models, one for HgSe clusters in Nd-Y and the other one for HgSe one-dimensional nanostructures in LTL, combining the results of the techniques above to yield intracluster structures of these semiconductor nanoclusters, as organized in zeolite pores.

II. ANOMALOUS X-RAY SCATTERING

Conventional powder diffraction is a very successful technique for both qualitative and quantitative analyses of most materials.[22,23] However, this method sometimes faces difficulty in identifying individual chemical constituents, especially in relatively complicated multicomponent mixtures. Under these conditions, AXS can provide sufficient structural information to identify the individual constituents in the compound leading to a more accurate structure determination. AXS uses the anomalous dispersion terms of the atomic scattering factor [Eqs. (1)] to extract structural information,

$$f(Q,E) = f^{\circ}(Q) + f'(E) + if''(E), \tag{1}$$

where E is the x-ray energy,

$$Q = 4\pi \sin(\theta)/\lambda. \tag{2}$$

Each element has its own characteristic threshold excitation energies (Fig. 1). At these energies, atoms absorb x-ray energy and electronic transitions between filled and empty shells occur. As a result, the dispersion terms of the atomic scattering factor, which represent the absorption and the resulting fluorescence, change dramatically. Therefore, the Bragg intensity, which is proportional to $|f(Q,E)|^2$, changes.

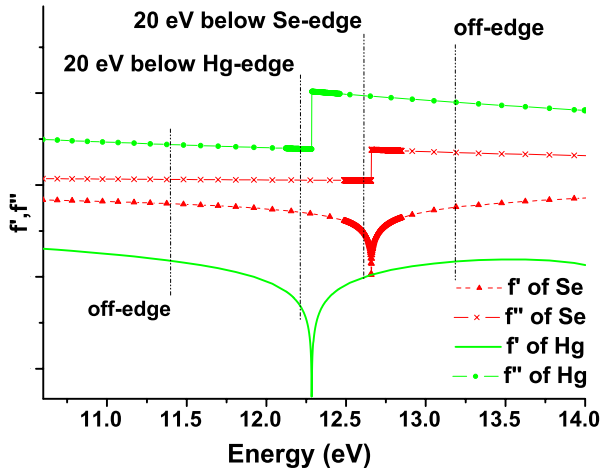

FIG. 1. (Color online) Variation of f' and f'' of Se and Hg at the Se K edge and Hg L edge, respectively. (These energies were chosen for our experiment.)

In general, this change is predominant at K and L absorption edges.[33] Exploiting the intensity difference between x-ray diffraction patterns collected at the vicinity (−20 eV) of an absorption edge and far (couple of hundreds of eV away) from an absorption edge, the identity of a particular element can ideally be made. The energy tunability of a synchrotron facility is required for the AXS experiments.

III. RESULTS AND DISCUSSION

A. Nanocluster synthesis

Hydrated forms of zeolites, LTL and Na-Y, i.e., $K_9(H_2O)_xSi_{27}Al_9O_{72}$ and $Na_{56}(H_2O)_xSi_{136}Al_{56}O_{384}$ (from Zeolyst), respectively, were used for our study. The effective volume of the channels of LTL is free of cations and can be used for the nanocluster fabrication followed by dehydration. However, in Na-Y, extra-framework cations (Na^+) occupy sites SI, SIV, and SV,[24] blocking the main cage. An ionic exchange was performed on Na-Y to remove Na^+ from the main cavities and to limit the resulting Nd^{3+} to SI and SI′ sites[24] according to the method described below. 10 g of Na-Y was stirred in a 500 ml solution of 0.1M $NdNO_3$ for 24 h. The resulting Nd-Y was recovered via filtration. Then, Nd-Y was washed with distilled water several times, and it was allowed to dry in air for several hours. After repeating the same procedure three times, EDX (energy dispersive x-ray analysis) measurements conformed the complete removal of Na^+ from the host. Next, both types of zeolites, Nd-Y and LTL, were dried in quartz tubes for 24 h at 500 °C in air. Then, the open ends of the quartz tubes were connected to a vacuum line and the temperature was raised to 550 °C. After 24 h of heating in the vacuum line, tubes were sealed and transferred to a dry box for nanocluster fabrication. Using scanning electron microscopy (SEM), the individual zeolite particles were determined to be 2500–5000 Å.

The dehydrated zeolite crystals were then sealed together with pure Se into a Pyrex tube at a vacuum of 20 mTorr. Next, Se was introduced into the channels and cages by

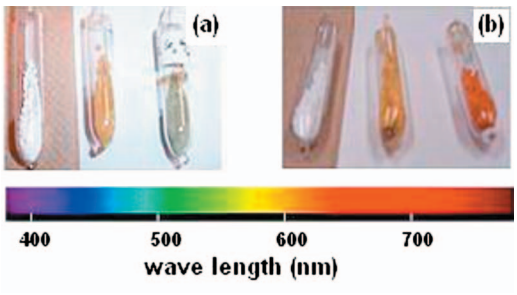

FIG. 2. (Color) Optical spectrum in comparison with the sample color. (a) From left, LTL, LTL/Se, LTL/HgSe. (b) From left, NdY, NdY/Se, NdY/HgSe. Our samples shows a blueshift in color with decreasing particle size, which indicates a decrease in optical band gap. On the nanoscale, the semiconductor band gap increases with the decreasing particle size. Therefore, the optical absorption wavelength changes.

chemical vapor deposition (CVD) at 360 °C for 48 h.[8] The resulting Nd-Y/Se ampoules were opened in the dry box and sealed together with Hg into a Pyrex tube at a vacuum of 20 mTorr. Finally, Hg was introduced into the compound by CVD at 160 °C for 24 h. The reaction stoichiometry was set to have the compositions LTL/$(HgSe)_4$ and NdY/$Hg_{30}Se_{32}$. The colors of our samples are presented in comparison with the optical spectrum in Fig. 2.

Initial XRD (using Cu radiation), optical absorption studies, and TGA were done at the University of Houston chemistry department. Raman spectroscopy and SEM studies were done at the Texas Center of Superconductivity. All of our AXS data sets were collected at the beamline X7A, National Synchrotron Light Source (NSLS), Brookhaven National Laboratory (BNL). For each sample, XRD patterns were recorded at the vicinity (−20 eV) of both Hg L and Se K absorption edges and far (±200 eV) from the absorption edges. X-ray diffraction patterns were recorded on empty zeolite samples at the off-edge energy as a reference.

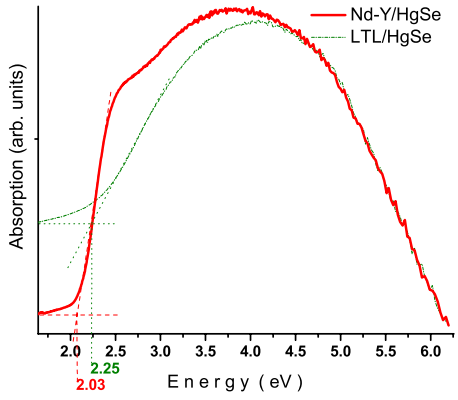

FIG. 3. (Color online) Comparison of LTL/HgSe and Nd-Y/HgSe absorption spectra. Estimated band gap for the HgSe nanoclusters in LTL (contain ~7.1 Å diameter channels) and NdY (contain ~13 Å diameter cages) zeolites are 2.25 and 2.03 eV, respectively.

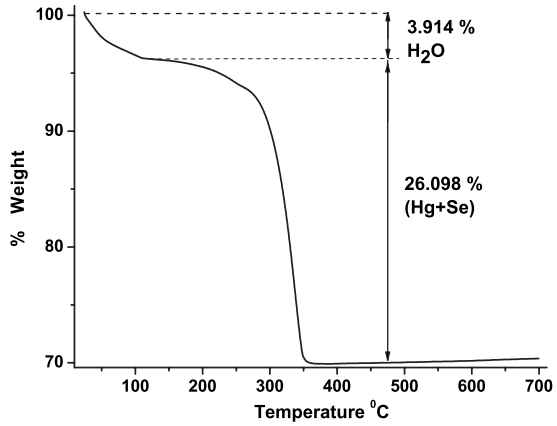

FIG. 4. TGA results of LTL/HgSe.

B. Optical absorption measurements

The absorption spectra were plotted in terms of $F(R)$, the Kubelka-Munk function. The diffuse reflectance R of the sample is related to the Kubelka-Munk function by Eq. (3), where K is the absorption coefficient and S is the scattering coefficient,

$$F(R) = (1-R)^2/(2R) = K/S. \quad (3)$$

Band gaps of the incorporated nanoclusters were estimated using optical absorption spectra (Fig. 3). We observed a clear increase in band gap with decreasing particle size obeying the size quantization effect.[25,26]

C. Thermogravimetric analysis

TGA plots were used to estimate the amount of water and Hg+Se (weight percentage) in the samples. In both LTL/HgSe (Fig. 4) and NdY/HgSe (Fig. 5) TGAs, the sharp drop of the curve from ~24 to 120 °C occurs due to the evaporation of water. The curve becomes very steep from 300 to 360 °C and thereafter it becomes flat, indicating the complete removal of Hg and Se from the host (this was confirmed by XRD of the residues). During this time, samples changed their color from dark orange (LTL/HgSe) or green

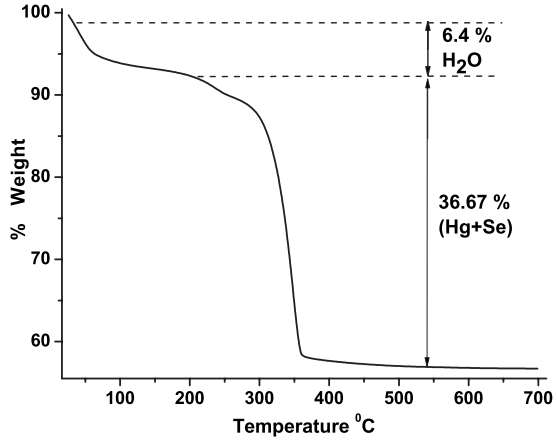

FIG. 5. TGA results of Nd-Y/HgSe.

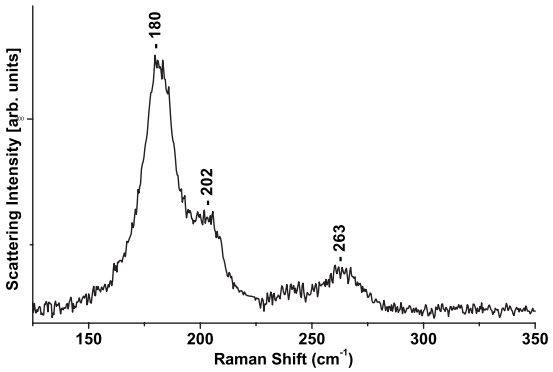

FIG. 6. Raman spectrum of LTL/HgSe.

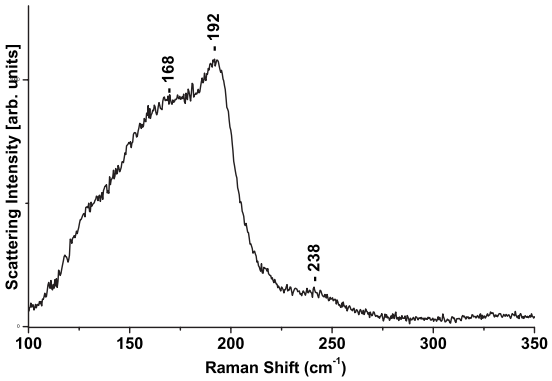

FIG. 8. Raman spectrum of NdY/HgSe.

(NdYHgSe) to pure white. Since zeolite decomposes at higher temperatures, we do not expect to see any drop in weight from 360 to 700 °C. Weights of the samples were noted before and after running TGA and the composition of Hg, Se, and H_2O was estimated using the percentage weight loss. The estimated compositions were used to apply initial occupational constraints in the Rietveld refinement.

D. Raman spectroscopy

The Raman spectra were obtained with 488 nm excitation using a Jobin Yvon Raman spectrometer equipped with a microscope and a liquid nitrogen cooled charge-coupled device detector. For both systems, the Raman spectra of filled zeolite were much stronger than those of the empty zeolite. The laser power density on the sample was kept extremely low to avoid overheating. The Raman spectra remained the same after long illumination, indicating that 488 nm excitation did not result in photoinduced structural changes. In the Raman spectra of LTL/HgSe, three peaks are clearly pronounced at 180, 202, and 263 cm^{-1} (Fig. 6). For comparison, the Raman spectrum of Se-incorporated LTL, exhibiting a single peak at 263 cm^{-1}, is also shown in Fig. 7. Similar Raman peak at 263 cm^{-1} has been reported earlier for Se-incorporated $AlPO_4^{-5}$ single crystals.[4,7] Since the dimensions of LTL and $AlPO_4^{-5}$ channels are very close, the 263 cm^{-1} peak can unambiguously be assigned to Se in the LTL channels. The Raman features at 180 and 202 cm^{-1}, which are absent for empty zeolite and LTL/Se, cannot be associated with either bulk Se or HgSe (they do not correspond to the bulk HgSe Raman peaks). This suggest that they originate from the unique HgSe nanostructure which differs in the two zeolites studied.

Figures 8 and 9 show the Raman spectra of Nd-Y/HgSe and Nd-Y/Se systems. Similarly to LTL/HgSe, the peaks at 168 and 192 cm^{-1} for Nd-Y/HgSe (Fig. 8) can be associated with the formation of Hg-Se nanoclusters in the pores of Nd-Y, whereas the peak near 238 cm^{-1} can be assigned to disordered Se chains[16] or polyselenide anions such as Se_2^{-2}.[17]

E. X-ray diffraction and Rietveld refinement

General remarks

LTL and Nd-Y zeolites have well-organized structures without any significant disorder.[27–31] Therefore, Bragg reflections are well resolved and sharp, and they are not accompanied by a diffuse scattering background (Figs. 10 and 11). Peak positions obey *P*6/*mmm* and *Fd*-3*m* space group symmetries, respectively. Hydration can change these Bragg intensities without introducing a significant diffuse scattering background.

Diffraction patterns taken at the off-edge energy after the encapsulation of Hg and Se are given in Figs. 12(a) and

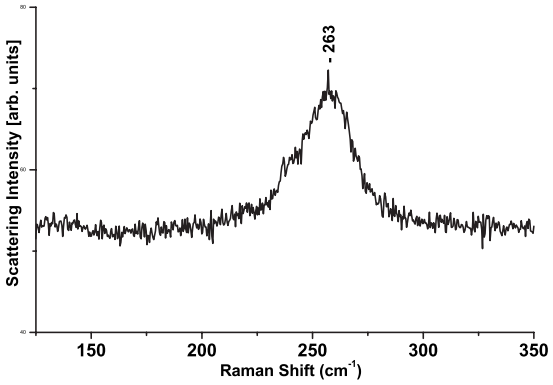

FIG. 7. Raman spectrum of LTL/Se.

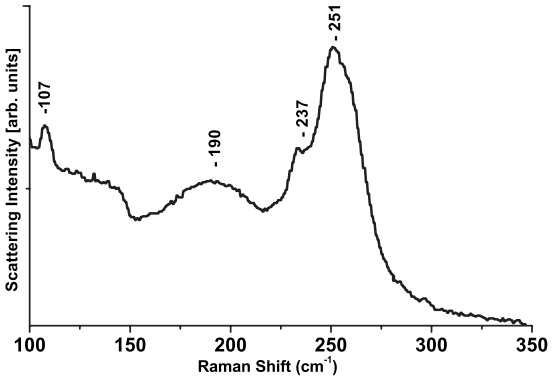

FIG. 9. Raman spectrum of NdY/Se. Data digitized from Ref. 16.

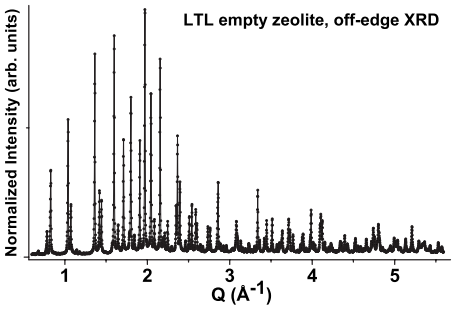

FIG. 10. XRD pattern of LTL empty host.

13(a). One remarkable feature in these XRD patterns is the pronounced diffuse scattering under the Bragg peaks,[27–31] shown in the insets of these figures. This may occur as a result of disorder within the nanocluster representing deviations from the *average* structure obtained by the Rietveld analysis.

F. Rietveld refinement

1. Off-edge data refinement

Initially, two models were refined against off-edge data sets of both LTL and NdY host zeolites. The refined atomic coordinates were used as initial models for the HgSe-encapsulated zeolite x-ray data refinement. Hg and Se atoms were located using Fourier electron density maps and Patterson methods. Initially, occupancies of the Hg and Se sites were constrained according to the reaction stoichiometry and the TGA results. However, at the last stage of the refinement, atomic coordinates (of both zeolite host and Hg/Se sites), occupancies, isotropic thermal displacement parameters, zero shift, background, and the profile parameters were refined simultaneously to optimize the quality of the fittings and the models. A shifted Chebyschev polynomial was fitted to the diffuse background which then was subtracted for the Rietveld refinement.

2. Anomalous x-ray scattering data refinement

At this stage, the structural models obtained for each zeolite/HgSe system from the off-edge data were simultaneously refined against all three data sets, Hg *L* edge-

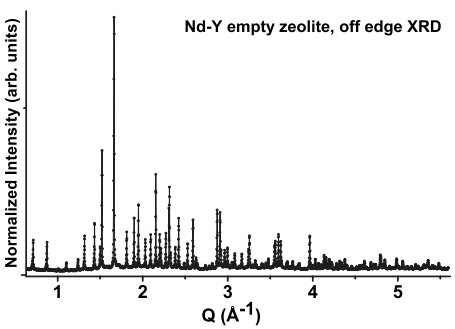

FIG. 11. XRD pattern of NdY empty host collected at off-edge energy.

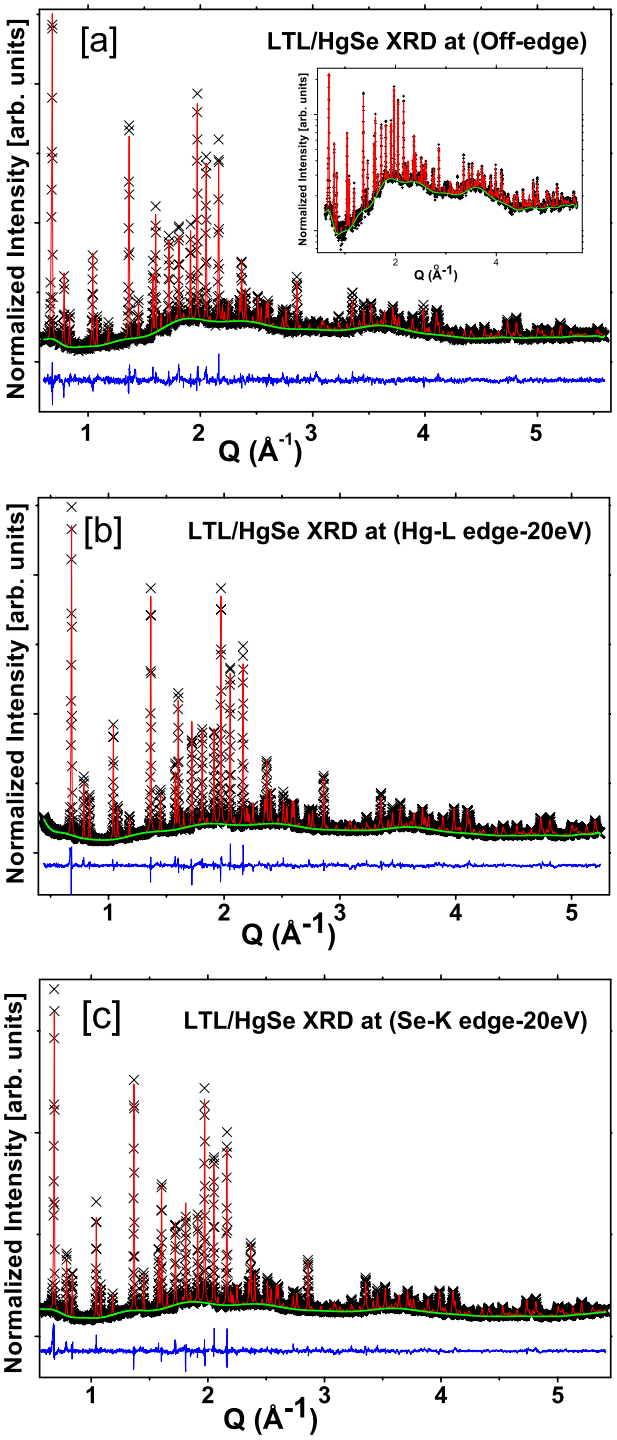

FIG. 12. (Color online) (a) The Rietveld fit to the powder pattern of the LTL/HgSe system collected at off-edge energy. Goodness of fit, R_{wp}=0.0635, R_p=0.04782, and R_{F^2}=0.1330. (b) The Rietveld fit to the powder pattern of the LTL/HgSe system collected at Hg *L* edge-20 keV. Goodness of fit, R_{wp}=0.0496, R_p=0.0372, and R_{F^2}=0.1061. (c) The Rietveld fit to the powder pattern of the LTL/HgSe system collected at Se *L* edge-20 keV. Goodness of fit, R_{wp}=0.0495, R_p=0.0365, and R_{F^2}=0.0825. Plots show the observed (×) and calculated (−) powder patterns with a difference curve at the bottom of each diagram. The overall χ^2 for (a), (b), and (c) is 2.818.

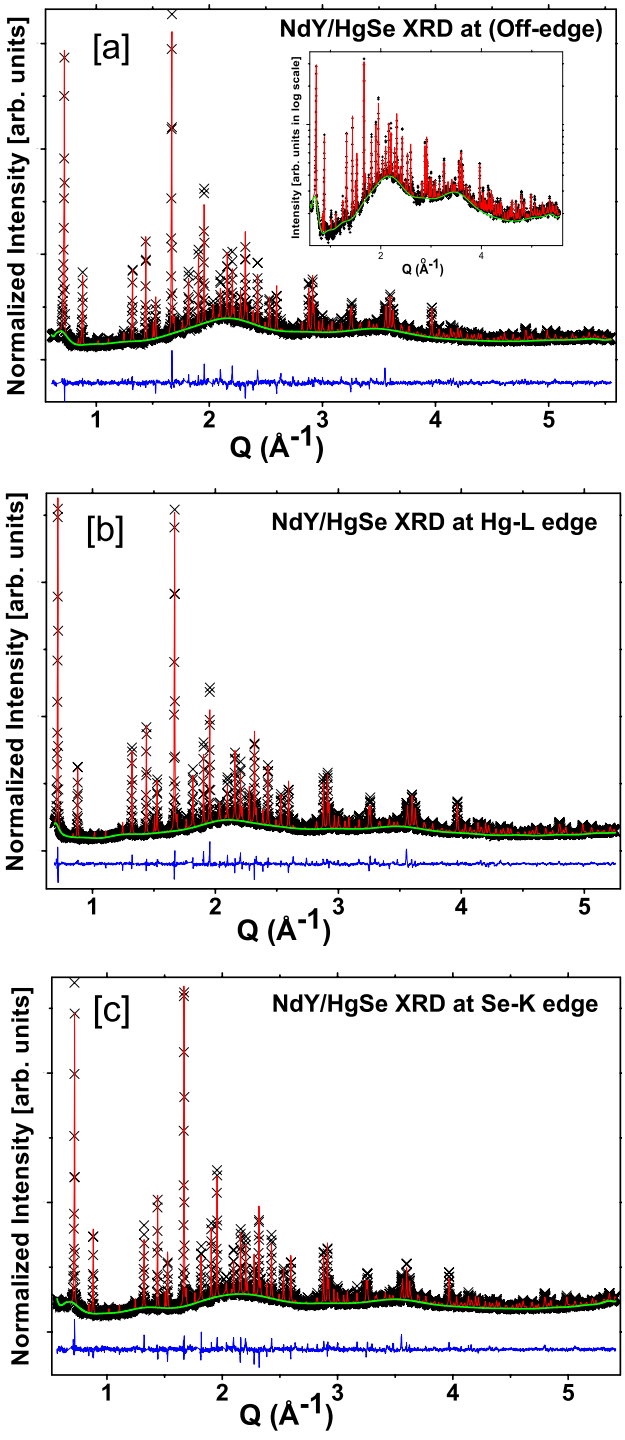

FIG. 13. (Color online) (a) The Rietveld fit to the powder pattern of the Nd-Y/HgSe system collected at off-edge energy. Goodness of fit, R_{wp}=0.0552, R_p=0.0416, and R_{F^2}=0.1291. (b) The Rietveld fit to the powder pattern of the Nd-Y/HgSe system collected at Hg *L* edge-20 keV. Goodness of fit, R_{wp}=0.0503, R_p=0.0362, and R_{F^2}=0.1115. (c) The Rietveld fit to the powder pattern of the Nd-Y/HgSe system collected at Se *L* edge-20 keV. Goodness of fit, R_{wp}=0.0519, R_p=0.0380, and R_{F^2}=0.1453. Plots show the observed (×), and calculated (−) powder patterns with a difference curve at the bottom of each diagram. The overall χ^2 for (a), (b), and (c) is 0.7845.

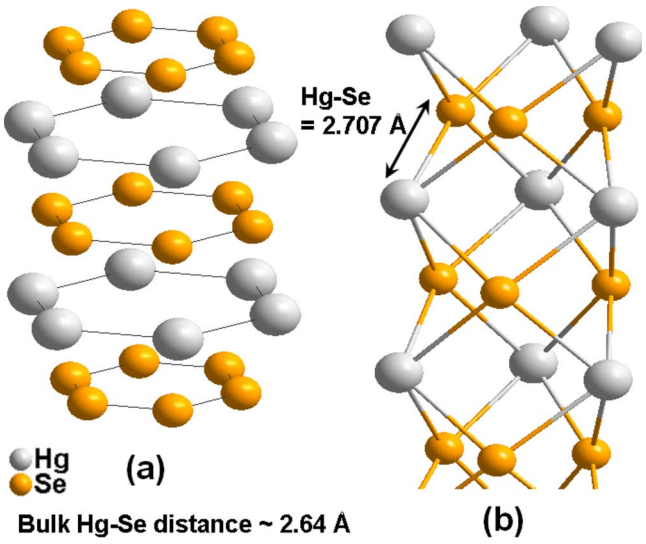

FIG. 14. (Color online) Proposed structural model for the nanocluster in LTL channels. (a) The resultant atomic positions from the refinement; each refined Se and Hg site has 6 and 12 equal positions, respectively, in the channel. However, the refined occupancy, which agreed well with the reaction stoichiometry, TGA results, and the interatomic distances, does not permit the existence of atoms at all equal positions. (b) is chemically the most favorable *average* structural model for the HgSe nanocluster for this atomic arrangement.

20 keV, Se *K* edge-20 keV, and off-edge introducing corresponding f' and f'' values.[32] Since the anomalous contrast (at the near-edge data sets) of the atomic structure factor contributes to the Bragg peak intensities, it was possible to optimize the quality of the final model (interatomic distances and angles) at this stage. Figures 12 and 13 present the Rietveld fits obtained from the AXS data refinement. The quality of fittings are acceptable, as described in Figs. 12 and 13.

Refined structural models are presented in Figs. 14 and 15. In both zeolites, the framework structure shows small changes in bond lengths and angles after incorporation of HgSe in the pores. However, a slight deformation was expected due to the influence of the heavy atoms, Hg and Se. The refined lattice parameters, $a=b=18.381\,51(21)$ Å and $c=7.491\,82(10)$ Å, of the LTL/HgSe system show ~0.05 Å expansion in *a* and *b* directions and a contraction of ~−0.02 Å in the *c* direction with respect to the lattice parameters of the empty LTL. The atomic arrangement obeys $P6/mmm$ symmetry as with the empty LTL. The refined composition, $Si_{27}Al_9O_{72}K_{7.6}(H_2O)_{11.124}(HgSe)_4$, agrees well with the reaction stoichiometry. There are no other major changes observed in the framework due to the incorporation of Hg and Se. Se-Hg distances (Table I) are reliable and close to the bulk Hg-Se distance (2.64 Å). Refined U_{iso} (isotropic thermal parameter) for the H_2O sites are higher mostly due to the statistical disorder associated with these sites (Table II). The same reason applies for the higher U_{iso} values of the Hg and Se sites. According to the reaction stoichiometry which agrees well with the refined site occupancy, all refined symmetrical positions cannot be filled. This causes the lattice relaxation of the filled sites to result in a statistical

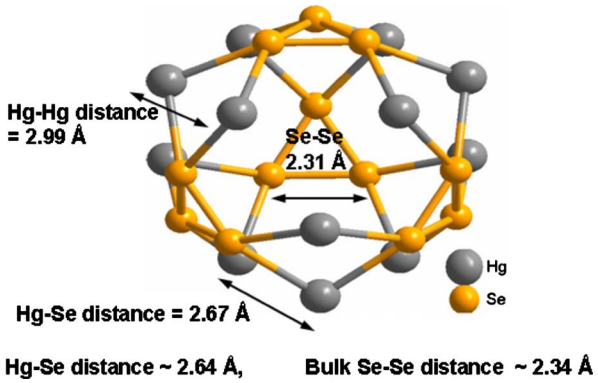

FIG. 15. (Color online) Proposed structural model for the HgSe nanocluster in the pores of Nd-Y. Refined atomic sites, Hg1, Se1, and Se2 (Table IV), each has 96 equal positions in the unit cell. The unit cell of Nd-Y contain eight big cages. Therefore, each site has 12 equal positions in a cage. The Se1 site has 32 equal positions in the unit cell and hence 4 equal positions in each cage. However, according to the reaction stoichiometry (which agrees well with the refined atomic fractions), only 1/3 of this sites can be filled. If we assume the full occupancy in a cage, only 2.5 cages are filled out of 8 total in the unit cell. Here, we have presented the most chemically satisfactory *average* structural model, which agrees with the conditions above, for the nanocluster.

disorder which can be reflected in U_{iso} values. The fact that Hg sites have higher U_{iso} values with respect to Se sites can be associated with the higher atomic number (Z=80) of Hg. The atomic number of Se is 34. Since Hg is a larger atom, it can contribute to statistical disorder more effectively, i.e., it will produce larger displacements of its neighbors. This linear molecular structure is bonded to the framework through extra-framework oxygen atoms. In addition to the average HgSe clusters, we suggest a significant disorder within the cluster which contributes to the diffuse scattering. Our Raman studies showing Se-Se vibrations would strongly support this idea.

Similar to the LTL zeolite, the NdY framework also changes bond lengths and angles after the incorporation of the HgSe nanoclusters in the pores. The refined lattice parameter, 24.681 22(2) Å, shows an ~0.03 Å expansion with respect to the lattice parameters of the empty NdY. The atomic arrangement still obeys *Fd*-3*m* symmetry preserving the basic shape of the NdY framework. The refined composition, $Si_{139.5}Al_{52.4}O_{384}Nd_{22.9}(H_2O)_{101.5}Hg_{28.8}Se_{31.92}$, well agrees with the reaction stoichiometry. There are no other major changes observed in the framework due to the incorporation of Hg and Se. In the HgSe structure, Se-Hg and Se-Se distances (Table III) are reasonable and close to the bulk Se-Se distance (2.34 Å) and bulk Hg-Se distance (2.64 Å). This average molecular structure is weakly bonded to the framework through extra-framework oxygen atoms. The explanation of the higher U_{iso} values in the Nd-Y/HgSe system (Table IV) is equally valid for the LTL/HgSe system, namely, that there is a measurable static disorder within the molecule due to the incomplete filling and defects within the molecular clusters.

IV. CONCLUSION

We presented a detailed structural model for the incorporated nanoclusters in the pores of each type of zeolite, LTL and Nd-Y. To the best of our knowledge, this is the first detailed structural study done on Nd-Y/HgSe and LTL/HgSe systems. A synthesis method was used to prepare compositionally well-defined samples which were shown to contain HgSe nanoparticles within the zeolite channels. We did not observe any HgSe bulk phase peaks in XRD patterns. However, large intensity changes for the zeolite Bragg peaks were

TABLE I. Selected bond lengths and angles in the refined LTL/HgSe structure. Standard deviations of 1-sigma are indicated in the parentheses.

Atom 1	Atom 2	Distance (Å)	Atom 1	Atom 2	Atom 3	Angle (deg)
Si1	O1	1.651(5)	O1	Si1	O4	110.58(28)
Si1	O2	1.6515(28)	O2	Si1	O4	112.66(29)
Si1	O4	1.674(4)	O4	Si1	O4	103.81(32)
Si2	O3	1.691(4)	O3	Si2	O4	112.92(24)
Si2	O4	1.549(5)	O3	Si2	O5	104.1(4)
Si2	O5	1.6713(23)	O3	Si2	O6	113.51(28)
Si2	O6	1.6387(25)	O4	Si2	O5	106.30(23)
Si (Avg.)	O (Avg.)	1.6647	O4	Si2	O6	107.69(32)
Hg1	Se2	2.83032(2)	O5	Si2	O6	112.14(29)
Hg1	Se3	2.70734(2)	Si1	O1	Si1	127.1(7)
			Si1	O2	Si1	146.2(8)
			Si2	O3	Si2	135.4(4)
			Si1	O4	Si2	146.1(4)
			Si2	O5	Si2	142.1(4)
			Si2	O6	Si2	147.6(4)

TABLE II. Refined atomic coordinates, occupancy, and thermal parameters of the LTL/HgSe structure. Standard deviations of 1-sigma are indicated in the parentheses.

Name	x/a	y/b	z/c	Mul.[a]	Occ.[b]	U_{iso} (Å)
Si(1)	0.0937(2)	0.3587(2)	0.5000	12	0.7500	0.0351(16)
Si(2)	0.1625(2)	0.4951(2)	0.2010(2)	24	0.7500	0.0236(8)
Al(1)	0.0938(2)	0.3587(2)	0.5000	12	0.2500	0.0351(16)
Al(2)	0.1625(2)	0.4952(2)	0.2010(16)	24	0.2500	0.0236(8)
O(1)	0.0000	0.2721(6)	0.5000	6	1.0000	0.0351(16)
O(2)	0.1632(3)	0.3264(6)	0.5000	6	1.0000	0.0236(8)
O(3)	0.2650(2)	0.5300(4)	0.2511(9)	12	1.0000	0.0187(38)
O(4)	0.1025(2)	0.4177(3)	0.3263(5)	24	1.0000	0.0147(38)
O(5)	0.4259(2)	0.8518(4)	0.2743(8)	12	1.0000	0.0186(31)
O(6)	0.1368(4)	0.4689(4)	0.0000	12	1.0000	0.0330(28)
K(1)	0.0000	0.3182(6)	0.0000	6	0.5038	0.0152(34)
K(2)	0.3333	0.6667	0.5000	2	0.9810	0.0258(30)
K(3)	0.0000	0.5000	0.5000	3	0.8685	0.0220(26)
Hg	0.1239(1)	0.0000	0.2442(3)	12	0.3333	0.561(7)
Se(1)	0.1000(25)	0.0000	0.5000	6	0.3333	0.171(7)
Se(2)	0.0872(3)	0.0000	0.0000	6	0.3333	0.168(6)
$H_2O(1)$	0.0874(4)	0.1748(8)	0.5000	6	0.4104(24)	0.276(10)
$H_2O(2)$	0.1040(3)	0.2028(1)	0.1532(14)	12	0.416(3)	0.368(10)
$H_2O(3)$	0.1404(42)	0.2809(8)	0.0000	6	0.333(38)	0.103(8)
$H_2O(4)$	0.0000	0.2720(15)	0.0000	6	0.281(6)	0.307(17)

[a]Site multiplicity.
[b]Site occupancy.

observed upon the addition of HgSe, which suggest that Hg and Se take well-defined positions inside the zeolite cages. The absence of bulk phase HgSe diffraction peaks also confirms the confinement of HgSe in their zeolite frameworks. Furthermore, the observed changes in optical properties are consistent with those expected from constraining the HgSe nanoparticle size by the different channel sizes in Nd-Y and LTL; the narrower cluster in LTL is more blueshifted than the average cluster in NdY.

Rietveld analysis of the Nd-Y, LTL, Nd-Y/HgSe, and LTL/HgSe structures were performed using the off-edge x-ray diffraction data sets and two near-edge data sets. The basic symmetries of the frameworks showed only minimal changes in the lattice parameters, bond lengths, and angles

TABLE III. Selected bond lengths and angles in the refined Nd-Y/HgSe structure. Standard deviations of 1-sigma are indicated in the parentheses.

Atom 1	Atom 2	Distance (Å)	Atom 1	Atom 2	Atom 3	Angle (deg)
Si/Al	O1	1.614(5)	O1	Si/Al	O2	114.34(31)
Si/Al	O2	1.6529(24)	O1	Si/Al	O3	110.57(31)
Si/Al	O3	1.6400(9)	O1	Si/Al	O4	108.85(35)
Si/Al	O4	1.6376(27)	O2	Si/Al	O3	98.70(32)
Si/Al	O (Avg.)	1.636	O2	Si/Al	O4	111.6(4)
Nd1	O3	2.009(7)	O3	Si/Al	O4	112.5(4)
Nd2	O2	2.663(8)	O (Avg.)	Si/Al	O (Avg.)	109.4
Nd2	O3	2.880(7)	Si/Al	O1	Si/Al	139.6(5)
Se2	Hg2	2.670(4)	Si/Al	O2	Si/Al	151.2(6)
Se2	Se1	2.31409(1)	Si/Al	O3	Si/Al	136.6(4)
Se2	Se2	2.03308(1)	Si/Al	O4	Si/Al	142.5(5)
Hg2	Hg1	2.998(10)	Si/Al	O (Avg.)	Si/Al	142.5

TABLE IV. Refined atomic coordinates, occupancy, and thermal parameters of the NdY/HgSe structure. Standard deviations of 1-sigma are indicated in the parentheses.

Name	x/a	y/b	z/c	Mul.[a]	Occ.[b]	U_{iso} (Å)
Si	0.9448(1)	0.1275(1)	0.0342(1)	192	0.7268	0.0187(9)
Al	0.9448(1)	0.1275(1)	0.0342(1)	192	0.2732	0.0187(9)
O (1)	0.8930(2)	0.0000	0.1070(2)	96	1.0000	0.0434(15)
O (2)	0.0054(2)	0.0054(2)	0.1285(3)	96	1.0000	0.0434(15)
O (3)	0.9536(3)	0.0790(2)	0.0790(2)	96	1.0000	0.0434(15)
O (4)	0.9322(3)	0.0648(2)	0.1852(2)	96	1.0000	0.0434(15)
Nd(1)	0.0000	0.0000	0.0000	16	0.1200(24)	0.0254(6)
Nd(2)	0.0681(1)	0.0681(1)	0.0681(1)	32	0.6584(24)	0.0254(6)
$H_2O(1)$	0.1532(6)	0.1532(6)	0.1532(6)	32	0.765(38)	0.124(9)
$H_2O(2)$	0.0357(7)	0.0668(6)	0.1217(5)	192	0.399(6)	0.124(9)
Hg(1)	–0.0123(3)	0.5875(3)	–0.0123(3)	96	0.1515(3)	0.343(5)
Hg(2)	0.0841(2)	0.4801(4)	0.0841(2)	96	0.1501(37)	0.343(5)
Se(1)	0.3400	0.3400	0.3400	32	0.3100(14)	0.168(5)
Se(2)	0.0045	0.5628(2)	0.1872(2)	96	0.2292(14)	0.168(5)

[a]Site multiplicity.
[b]Site occupancy.

following the incorporation of the semiconductor nanoclusters. No zeolite symmetry change was observed and the peaks remain sharp. Structural models were developed for each of the two systems. In the most chemically satisfactory model of the LTL/HgSe system, which agrees with all of the experimental data, Hg is coordinated by two Se atoms at distances of ~2.8 and ~2.7 Å, and Se by two Hg atoms at the same distances. In the most chemically satisfactory model of the NdY/HgSe system which agrees with all of the experimental data, Hg is coordinated by two Se atoms at a distance of ~2.67 Å, and Se by two Hg atoms and two Se atoms at distances of ~2.67 and ~2.31 Å, respectively. In both cases, these average molecular structures are bonded to the framework oxygen atoms weakly through Hg atoms preventing the complete rotational freedom of these encapsulated species. The average structural model for the clusters in LTL is significantly different from that in Nd-Y reflecting the difference in both pore dimensions and geometry. The proposed models for the HgSe cluster both differ from the bulk HgSe structure (different symmetry than the bulk and 2%–10% change in bond lengths). It should be emphasized that our structural refinement yields the average molecular structure in both cases. It is our strong belief that the *individual* clusters possess substantial deviations or replacive disorder and/or rotational disorder from the two average structures.

Both Nd-Y/HgSe and LTL/HgSe samples showed well pronounced characteristics in the Raman spectra which are clearly absent in the Raman spectra of empty zeolites and differ from those of bulk HgSe. Characteristic Raman features from Se-Se bonds in the LTL/HgSe system are assumed to be due to the presence of disorder within both selenium and HgSe clusters. The Se-Se features were identified with the previous knowledge of $AlPO_4^{-5}$/Se single crystal system, confirming that there is a reasonable fraction of Se-Se bonds within the nanoclusters

The diffuse scattering associated with the above-noted molecular disorder is to be solved in the next phase of this project. In these measurements, we intend to perform PDF studies on the diffuse part of our zeolite/HgSe systems. A properly corrected synchrotron data set with sufficient resolution (both in energy and Q) collected up to a high Q value [Eq. (2)] will be Fourier transformed into real space coordinates to obtain the PDF of each nanocluster system. In order to do that, we have performed PDF measurements at the European Synchrotron Radiation Facility (ESRF) and are presently analyzing these data.

As mentioned elsewhere, $AlPO_4^{-5}$ consists of one dimensional channels which are very similar to the dimensions of the LTL channels. For a better understanding of the Raman spectra, we intend to grow HgSe nanostructures in the one-dimensional channels of $AlPO_4^{-5}$ single crystals. Qualitative x-ray structural studies of Se in $AlPO_4^{-5}$ single crystals (diffuse scattering associated with Se one-dimensional helical chain structures) have already been published by Li *et al.*[4] We intend to extend these measurements to Hg-Se and use diffractometer scans rather than photographic films.

ACKNOWLEDGMENTS

We thank the DOE/BES (Contract No. DE-FG02-04ER46160) for their extended financial support of this work and the Robert A. Welch Foundation. We also thank T. Vogt and Y. Lee at the (BNL/NSLS) for the use of the X7A beamline. Jim Meen at the Texas Center for Superconductivity at the University of Houston (TcSUH) performed SEM measurements, for which we thank him. This work is partly supported by the State of Texas through the Texas Center for Superconductivity at the University of Houston.

*Deceased.

[1] A. Rogach, S. Kershaw, M. Burt, M. Harrison, A. Kornowski, A. Eychmüller, and H. Weller, Adv. Mater. (Weinheim, Ger.) **11**, 552 (1999).

[2] X. Duan, Y. Huang, Y. Cui, J. Wang, and C. M. Lieber, Nature (London) **409**, 66 (2001).

[3] *Semiconductor and Metal Nanocrystals Synthesis and Electronic and Optical Properties*, edited by V. I. Klimov (Dekker, New York, 2004).

[4] I. L. Li, P. Launois, and Z. Tang, Appl. Surf. Sci. **226**, 36 (2004).

[5] A. Goldbach, M.-L. Saboungi, L. Iton, and D. L. Price, Chem. Commun. (Cambridge) **11**, 997 (1999).

[6] T. Egami and S. J. L. Billinge, *Underneath the Bragg Peaks: Structural Analysis of Complex Materials* (Elsevier, New York, 2003).

[7] V. V. Poborchii, A. V. Kolobov, J. Caro, V. V. Zhuravlev, and K. Tanaka, Phys. Rev. Lett. **82**, 1955 (1999).

[8] A. Goldbach, M. Grimsditch, L. Iton, and M.-L. Saboungi, J. Phys. Chem. B **101**, 330 (1997).

[9] A. Goldbach and M. L. Saboungi, Eur. Phys. J. E **12**, 185 (2003).

[10] V. N. Bogomolov, V. V. Poborchy, S. G. Romanov, and S. I. Shagin, J. Phys. C **18**, L313 (1985).

[11] S. J. L. Billinge, V. Petkov, and T. Proffen, Commission on Powder Diffraction of the International Union of Crystallography Newsletter, 2000, Vol. 24.

[12] S. Pramanik, S. Bandyopadhyay, and M. Cahay, 2003 Third IEEE Conference on Nanotechnology [Nanotechnology **2**, 87 (2003)] (IEEE-NANO, 2003).

[13] C. Lageweg, S. Cotofana, and S. Vassiliadis, 2003 Third IEEE Conference on Nanotechnology [Nanotechnology **2**, 449 (2003)] (IEEE-NANO, 2003).

[14] S. Noda, T. Asano, and M. Imada, 2003 Third IEEE Conference on Nanotechnology [Nanotechnology **2**, 277 (2003)] (IEEE-NANO, 2003).

[15] N. Hemon, Y. Wang, M. M. Eddy, G. D. Stucky, D. E. Cox, K. Moller, and T. Beid, J. Am. Chem. Soc. **111**, 530 (1989).

[16] P. Armand, M.-L. Saboungi, D. L. Price, L. Iton, C. Cramer, and M. Grimsditch, Phys. Rev. Lett. **79**, 2061 (1997).

[17] I. Goldbach, J. Jonson, D. Meisel, L. A Curtiss, and M. L. Saboungi, J. Am. Chem. Soc. **121**, 1461 (1999).

[18] A. L. Ankudinov, J. J. Rehra, J. J. Low, and S. R. Bare, J. Chem. Phys. **116**, 1911 (2002).

[19] T. Bein, MRS Bull. **30**, 713 (2005).

[20] G. Telbiz, O. Shvets, V. Vozny, and M. Brodyn, Stud. Surf. Sci. Catal. **135**, 325 (2002).

[21] A. Larson and R. V. Dreele, Los Alamos National Laboratory Technical Report No. LAUR 86–748, 1994 (unpublished).

[22] *Resonant Anomalous X-ray Scattering, Theory and Applications*, edited by G. Materlik, C. J. Sparks, and K. Fischer (North Holland, Amsterdam, 1994).

[23] Y. Waseda, *Anomalous X-Ray Scattering for Materials Characterization* (Springer, New York, 2002).

[24] J. G. Nery, M. V. Giotto, Y. P. Mascarenhas, D. Cardoso, F. M. Z. Zotin, and E. F. Sousa-Aguiar, Microporous Mesoporous Mater. **41**, 281 (2000).

[25] I. K. Akopyan, O. N. Volkova, and B. V. Novikov, Phys. Solid State **39**, 407 (1997).

[26] W. E. Buhro and V. L. Colvin, Nat. Mater. **2**, 138 (2003).

[27] I. Z. Association, Database of Zeolite Structures, 2000.

[28] R. M. Barrer and H. Villiger, Z. Kristallogr. **128**, 352 (1969).

[29] J. J. Hriljac, M. M. Eddy, A. K. Cheetham, J. A. Donohue, and G. J. Ray, J. Solid State Chem. **106**, 66 (1993).

[30] C. Baerlocher, W. Meier, and D. Olson, *Atlas of Zeolite Framework Types* (Elsevier, New York, 2001).

[31] M. Treacy and J. Higgins, *Collection of Simulated XRD Powder Patterns for Zeolites* (Elsevier, New York, 2001).

[32] D. E. Cox and A. P. Wilkinson, Brookhaven National Laboratory, Technical Report No. BNL-48626; CONF-930899–1 (1993).

[33] We should note that the Hg-L line shows only a small change in the scattering factor at low Q. However, at modest Q, the change becomes increasingly larger because the real part of the scattering factor is essentially Q independent.